2013

Influence of heat input on friction stir welding for the ODS steel MA596

Baker, B.W.; Brewer, L.N.; Menon, E.S.K.; McNelley, T.R.; El-Dasher, B.; Torres, S.; Farmer, J.C.; Mahoney, M.W.; Sanderson, S.

Minerals, Metal, and Materials Society

B.W. Baker, L.N. Brewer, E.S.K. Menon, T.R. McNelley, B. El-Dasher, S. Torres, J.C. Farmer, M.W. Mahoney, and S. Sanderson, Influence of heat input on friction stir welding for the ODS steel MA956," Friction Stir Welding VII, TMS 2013, p.127-138
http://hdl.handle.net/10945/55343

Friction Stir Welding VII
Edited by: Rajiv Mishra, Murray W. Mahoney, Yutaka Sato, Yuri Hovanski, and Ravi Verma
TMS (The Minerals, Metals, and Materials Society), 2013

INFLUENCE OF HEAT INPUT ON FRICTION STIR WELDING FOR THE ODS STEEL MA956

B.W. Baker[1], L.N. Brewer[1*], E.S.K. Menon[1], T.R. McNelley[1], B. El-Dasher[2], S. Torres[2], J.C. Farmer[2], M.W. Mahoney[3], and S. Sanderson[4]

[1]Naval Postgraduate School, Monterey, CA
[2]Lawrence Livermore National Laboratory, Livermore, CA
[3]Consultant, Salt Lake City, Utah
[4]MegaStir Technologies, Salt Lake City, Utah

Keywords: Friction Stir Welding, Oxide Dispersion Strengthened Steel, MA956

Abstract

The oxide dispersion strengthened steel MA956 was friction stir welded using eight different rotational speed/translational speed combinations using a polycrystalline cubic boron nitride tool. Weld parameter conditions with high thermal input produced defect-free, full penetration welds. Electron backscatter diffraction showed a significant increase in grain size in the stir zone, a body centered cubic torsional texture in the stir zone, and a sharp transition in grain size across the thermo-mechanically affected zone. Micro-indentation results showed an asymmetric reduction in hardness across the transverse section of the weld that was sensitive to the heat input. This change in hardness is explained by the increase in grain size and may be described using a Hall-Petch type relationship.

Introduction

Because of their high temperature strength, radiation damage resistance, creep resistance, and corrosion resistance, oxide dispersion strengthened (ODS) ferritic-martensitic (FM) steels are attractive candidates for high temperature power production applications including proposed fusion reactors[1] and fast breeder reactors[2]. FM steels experience far less radiation swelling than austenitic steels, and the addition of Y_2O_3 and other oxide dispersoids gives these materials exceptional high-temperature strength and creep resistance due to the pinning of grain boundaries and dislocations. The dispersed oxides also mitigate radiation swelling and embrittlement by providing sites for the accumulation of hydrogen and helium atoms. Although the thermo-mechanical and radiation resistance properties of ODS FM steels are promising, traditional fusion joining processes for these alloys such as gas tungsten arc and gas metal arc welding are ineffective due to agglomeration of the oxide particles during melting of the base metal. The resulting inhomogeneous distribution of the oxide particles significantly reduces strength in depleted areas[3, 4]. To preserve the strengthening capability of the dispersed oxides

* Correspondence should be addressed to lnbrewer@nps.edu

and high temperature creep resistance, friction stir welding (FSW) is a promising solid state joining method to join ODS steels for fusion or advanced energy production designs. Several authors have demonstrated the capability to join different ODS alloys via FSW with good success[5-10].

FSW was invented at The Welding Institute (TWI) of the United Kingdom in 1991 as a solid state joining technique[11]. A detailed review of process parameters, process modeling, microstructure evolution, material properties, and specific material issues for FSW has been completed by Mishra which focuses primarily although not exclusively on aluminum alloys[12]. Due to early limitations on tool materials, FSW was initially constrained to low melting temperatures alloys such as aluminum, magnesium, and lead. However, improvements in FSW tool materials such as the use of polycrystalline cubic boron nitride (PCBN) and W-Re pins have expanded the use of FSW to higher temperature alloys such as steels. Expanding the use of FSW to steels and polymers, Nandan provides a comprehensive review of heat generation, heat transfer and plastic flow, tool design, defect formation, and material properties for FSW applications[13].

Based on the current literature, increasing the heat input during FSW of MA956 is expected to increase the grain size in the stir zone (SZ) while consequently lowering hardness[5, 6, 8, 9]. The research results reported herein quantifies the heat input during FSW as a function of the tool rotational speed and tool traverse speed. The ratio of these terms has been analyzed as the pseudo-heat index by Mishra or weld pitch by Nandan and has been previously related to the formation of defects in the weld as well as grain growth in the SZ[12, 13]. This paper will demonstrate the effect of this pseudo-heat index upon the microstructure and properties of the friction stir weld microstructure in MA956.

Experimental Procedure

The material used in this study was MA956, a high Cr ferritic ODS steel with a measured material composition (Anamet Inc., inductively couple plasma-mass spectrometry) shown in Table I. MA956 was canned and extruded at 1100°C (2025°F) and subsequently hot-rolled in three passes at 1100°C (2025°F) over 4 hours with reheating to 1100°C (2025°F) for 30 minutes before and after each rolling pass before final machining into 4 mm (0.157 inch) thick plates.

Table I. Chemical Composition of MA956 (wt%)

C	Cr	Al	Ti	Y_2O_3	Mo	Mn	Ni	S	Si	P	Fe
0.023	19.93	4.75	0.39	0.51	0.02	0.09	0.04	0.008	0.08	0.006	Bal.

FSW of MA956 plate was accomplished by MegaStir Technologies using a convex step spiral scrolled shoulder (CS4) tool with an MS80 grade PCBN tip that requires no tool tilt. FSW parameters of tool rotation rate in revolutions per minute (RPM) and tool traverse speed in inches per minute (IPM) were varied to produce welds of differing quality and consolidation. Plunge force was maintained constant at 17.8 kN (4000 lbf).

Samples of friction stir welded MA956 plate were sectioned and analyzed by optical microscopy (OM), scanning electron microscopy (SEM), electron backscatter diffraction (EBSD), and micro-indentation. Cross sections across the weld path were metallographically prepared for each welding condition by standard metallographic preparation techniques with SiC papers, aluminum oxide polishing solutions, and 0.05 mm colloidal silica solution and electropolishing at 20 V using an electrolyte containing 10% perchloric acid in ethanol maintained at 250 K (-23 C). Microstructural examinations were conducted using a Zeiss Neon 40 field emission SEM at 20 keV. All EBSD analyses were carried out using the TSL OIM 6.0 system with a Hikari camera at 20 kV using a 60μm objective aperture with an approximate probe current of 1 nA. EBSD data was de-noised using TSL OIM software cleanup functions of grain dilation and grain confidence index standardization in accordance with recommended settings. To ensure an adequate number of grains were counted for pole figure analysis, data was collected from areas with minimum dimensions of 150x300 μm equating to a minimum of 2000 grains for the most limiting case. For areas of very fine grain size such as the base material (BM), a step size of 0.25 μm was used equating to over 20,000 grains in the analysis area. For other areas with a larger average grain size, a step size of 0.5 μm was used. Microhardness measurements were accomplished using a HVS-1000 microhardness tester with a diamond indenter and settings of 1 kg-force (2.2 lbf) load and a dwell time of 15 seconds. The hardness tester calibration was verified before and after indentation using a National Institute of Standards and Technology (NIST) certified specimen with a hardness of 726 HV and a certified error of 1.9%.

Results

Full penetration, defect free welds were observed for a range of FSW conditions with higher heat input (Table II and Figure 1). Heat input was quantified using the ratio of the rotational speed to the translational speed. Weld quality and penetration were determined by macrographs of the weld nugget as a function of RPM and IPM combinations in order to establish weld parameters to achieve defect free microstructures. Macroscopic metallographic observations are summarized in Table II. A higher heat input, i.e., increasing tool rotation rate or decreasing tool traverse speed, resulted in a defect free weld nugget. Defect free welds were produced when the ratio of rotational speed to translation speed was greater than 100 (Figure 1a). For conditions with heat input ratios less than 100, welds were observed to be defective with tunnel defects occurring at the bottom or edges of the SZ (Figure 1b).

Table II. Friction stir welding parameter summary.

Tool Rotation Rate (RPM)	Tool Traverse Speed (IPM)	RPM/IPM	Weld Quality	Weld Penetration
200	2	100	Lack of Consolidation	Incomplete
300	2	150	Defect Free	Full
300	4	75	Lack of Consolidation	Incomplete
300	6	50	Lack of Consolidation	Incomplete
400	2	200	Defect Free	Full
400	4	100	Defect Free	Full
400	7	57	Lack of Consolidation	Incomplete
500	1	500	Defect Free	Full

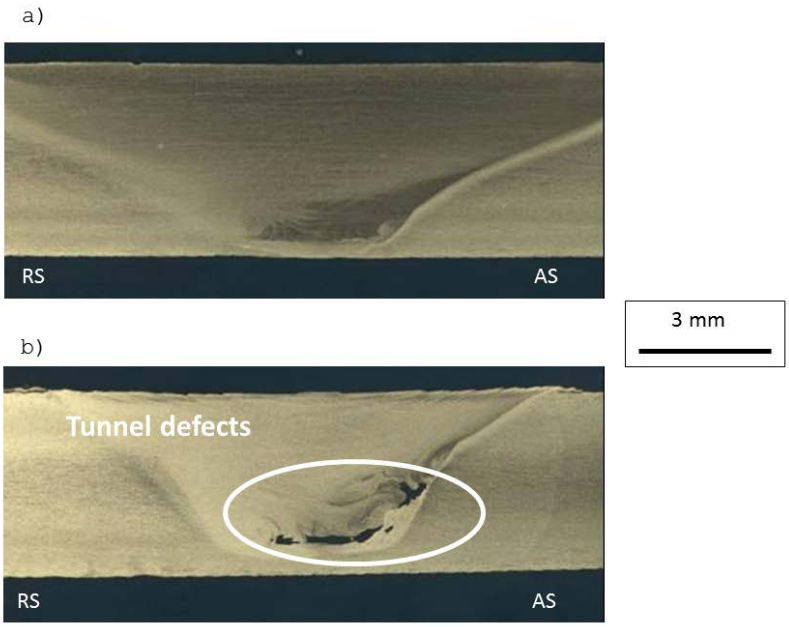

Figure 1. Optical macrographs of transverse metallographic cross-sections for (a) 400 RPM/2 IPM showing a full penetration defect free weld and (b) 400 RPM/7 IPM showing tunnel defect formation at a higher tool traverse rate. (RS=retreating side, AS=advancing side)

The grain size of the SZ increased systematically with increasing heat input (Table III). In all cases, the grain size in the stir zone was larger than the BM (Figure 2). The highest heat input (RPM/IPM=500) resulted in an order of magnitude increase in grain size compared with the BM. This observation is consistent with the previous work on similar ODS steels[5, 8]. The SZ grain size increased with increasing pseudo-heat index, but the relationship was non-linear.

Table III. SZ Hardness and SZ Grain Size Diameter for FSW parameter conditions.

FSW Condition	Mean SZ Grain Size Diameter (microns)	Mean SZ Hardness (HV)
BM	0.89	346 ± 6.6
275/4	1.5	248 ± 4.7
300/2	4.16	225 ± 4.3
400/4	6.94	221 ± 4.2
500/1	12.45	218 ± 4.2

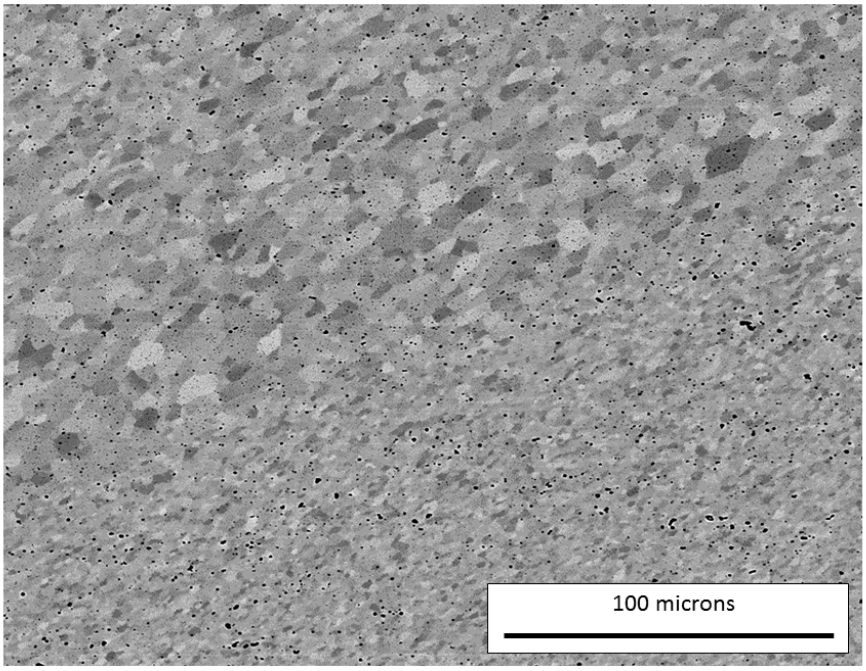

Figure 2. Backscatter SEM image of FSW MA956 with parameters of 400 RPM/4 IPM across SZ, TMAZ, and BM showing large change in grain size and little change in distribution of oxide particles.

In addition, electron microscopy for each FSW parameter combination showed a sharp transition in grain size across the thermo-mechanically affected zone (TMAZ) (Figure 2). This effect was most pronounced for high heat input conditions, particularly on the advancing side (AS) as opposed to the retreating side (RS). The most gradual grain size transition at the AS

TMAZ occurred for the 400 RPM/4 IPM combination, corresponding to the lowest heat input. However, the grain size gradients on the RS were less sharp and extended over the area of several orientation maps. Figure 3 is a composite representation of inverse pole figure (IPF) maps across the entire weld nugget.

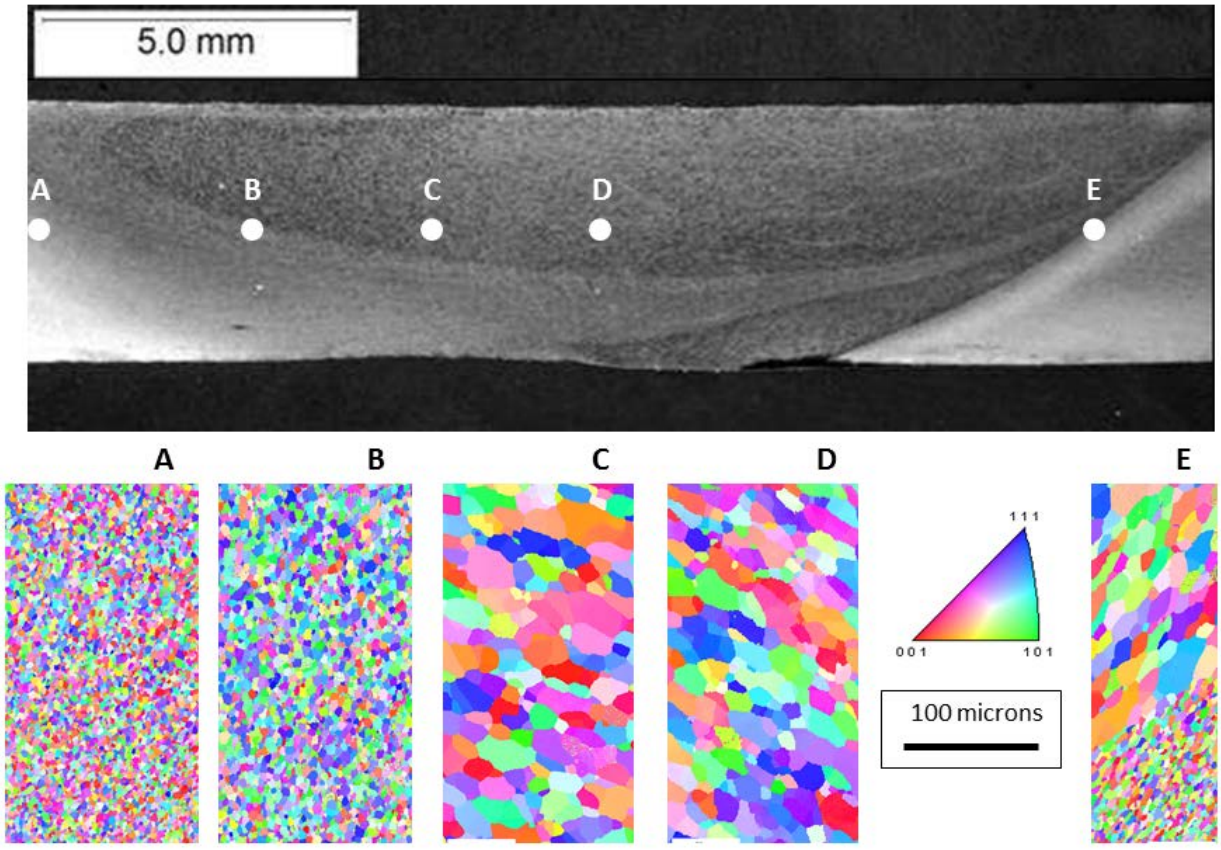

Figure 3. Representation of IPF maps across weld nugget for 500 RPM/1 IPM.

The microhardness in the welded microstructure varied significantly across the weld section and with the level of heat input. In addition, the hardness profiles were asymmetric across the weld nugget. The mean hardness decreased systematically in the SZ as the grain size increased (Table III). For all FSW combinations, the SZ hardness was substantially lower than the BM hardness. An example of the hardness profile is shown for the 500 RPM/1 IPM condition (Figure 4).

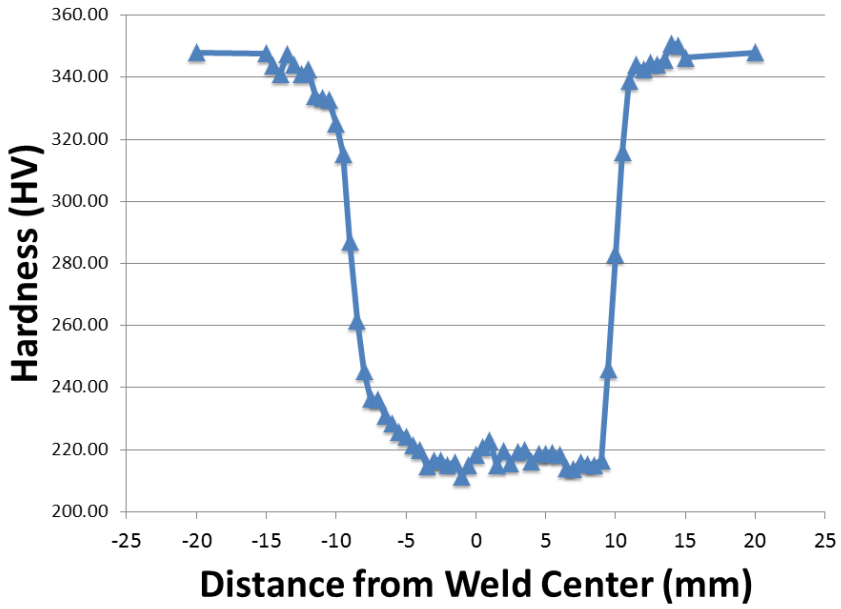

Figure 4. Hardness profile across the SZ for 500 RPM/1 IPM combination.

Pole figures for each FSW condition displayed a consistent torsional texture which is distinctly different from the rolling texture in the base material. The intensity did not change dramatically as heat input increased, but may have decreased slightly. Each FSW combination produced a persistent body centered cubic (BCC) torsional texture compared to the rolled texture of the BM as shown in Figure 5. Similar results have been shown for both torsional steel textures and FSW SZ textures for other ODS steels.[8, 14, 15]

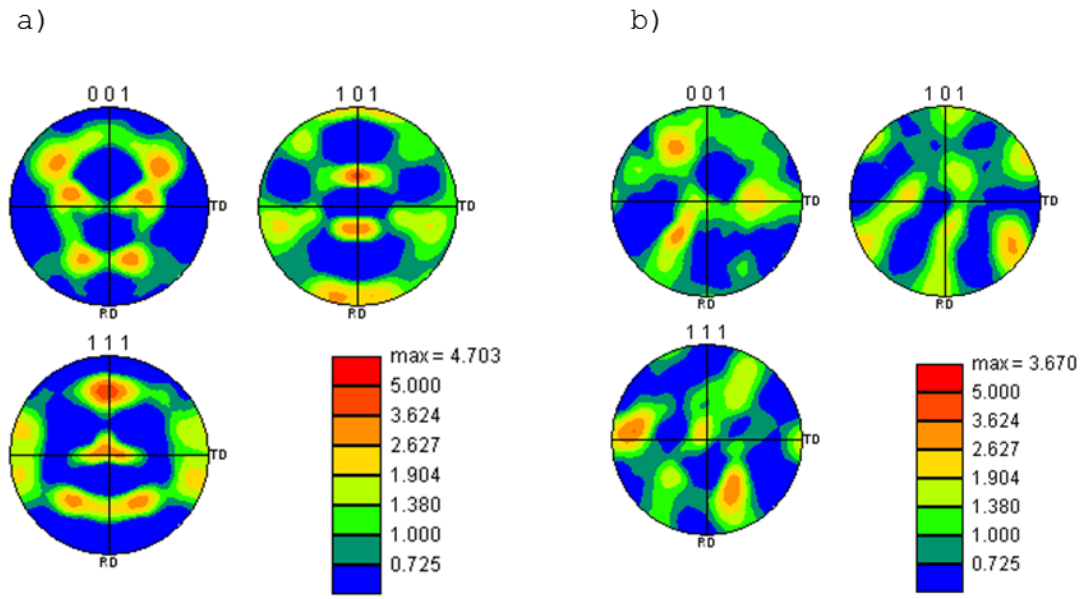

Figure 5. Pole figures for (a) BM rolled texture, and (b) 500 RPM/1 IPM BCC torsional texture.

Discussion

This works suggests that pseudo-heat index may be an effective way to estimate FSW conditions required for successful joining. As shown in the macrographs of Figure 1, weld defects systematically occurred for low heat input conditions, as described by the pseudo-heat index (RPM/IPM). This observed trend is similar to work by Chimbli who researched minimizing lack of consolidation defects in aluminum by varying FSW process parameters[16]. The ratio of tool rotation rate to tool traverse rate was found to be a good measure of the ability to form defect free consolidated welds. For MA956, the minimum range of pseudo-heat index that produced consolidated defect free welds was between 100 to 150. This concept is similar to research by Biswas in a review of FSW parameters on an aluminum alloy[17]. In this research, the overall mechanical response of the welded alloy depended on the ratio of tool rotational speed to tool traverse speed. For the aluminum alloy and tool material used, the suitable value of this ratio was between 380 to 400.

Quantifying heat input as the simple ratio between rotational and translation speed may not be sufficient for predicting the resultant friction stir weld microstructure. In this work, two FSW conditions with the same pseudo-heat index (400 RPM/4 IPM and 200 RPM/2 IPM) produced successful and defective welds, respectively. In very recent research by Wang et. al., MA956 with a coarser starting grain size (hundreds of microns) was friction stir welded with a high heat input (1000 RPM/2 IPM) [10]. Using the pseudo-heat index, this welding condition should apply the same heat input as the 500 RPM/1 IPM condition used in this work. However, the SZ grain size observed by Wang et al. is approximately 1-2μm, compared with the 12μm grain size observed in this work. This difference points out the importance of both the starting microstructure and the heat input model for predicting the SZ grain size. More elaborate heat input models [12, 13, 18] have been developed and should be applied to systematic studies connection FSW conditions with the starting and resultant microstructures.

The observed grain coarsening in the SZ is likely due to dynamic recrystallization. More typically, FSW results in grain refinement but in steels, and depending on the initial grain size, grain coarsening can occur. In a detailed review by Doherty et al. the term recrystallization is defined as the formation of new grain structures in a deformed material by the formation and migration of high angle grain boundaries driven by the stored energy of deformation and the term dynamic recrystallization is defined as the occurrence of recrystallization during deformation[19]. Based on these definitions, the term dynamic recrystallization is appropriate to describe the observed dramatic increase in grain size during FSW.

Micro-indentation results show that FSW reduces the hardness of the BM by approximately 37% compared to the SZ and that the hardness profile across the weld nugget is asymmetric, consistent with results from several authors[5, 6, 8]. Although the differences in SZ hardness between the varying FSW parameters conditions is small and is close to the accuracy of the hardness measurements, the average values of each set of SZ hardness measurements suggest that there is a systematic difference in hardness between the conditions that may be relatable to grain size. The relationship between grain size and hardness can be summarized as follows: (1) traversing from the SZ to the RS, the grain size gradually decreases and hardness gradually increases, (2) traversing from the SZ to the AS, the grain size and hardness are nearly constant until reaching the TMAZ at which point a very sharp decrease in grain size and increase in

hardness occurs, and (3) these effects are enhanced as the heat input increases, i.e., the SZ grain size increases and the abruptness of the transitions, both on the RS and most noticeably on the AS, is more distinct for higher heat input conditions. The change in grain size across the weld explains the asymmetric nature of the hardness profiles and at lower heat input values, the asymmetry is less noticeable.

Little change in micro-scale oxide particle distribution was observed for these microstructures for all FSW conditions. For example, no meaningful change in oxide particle size or distribution could be seen in backscattered electron images across the SZ/TMAZ interface for the 400 RPM/4 IPM condition, (Figure 2). It is well known that MA956 has both a micro-scale and a nano-scale oxide particle distribution and the results in this work cannot speak to changes in the nanoscale oxides[9, 20]. Atom probe tomography (APT) measurements by other authors have concluded that the oxide particle size and distribution does not change much during FSW[7].

The coupled increase in SZ grain size and reduction in SZ hardness with increasing heat input during FSW suggests that the Hall-Petch relationship may aptly describe the strengthening mechanism in the SZ. A plot of SZ hardness versus inverse square root of SZ grain size is shown in Figure 6 and shows a nearly linear relationship. The agreement of this hardness data suggests that much of the strength at low temperatures in the stir zone is controlled by the grain size; however, hardness is a function of both yield strength and work hardening. Tensile measurements that can separately measure the yield strength should clarify the strengthening mechanism in stir zone material. It should be noted that the hardness of the BM is much greater than for any of the SZ microstructures, and it does not lie on the Hall-Petch line, suggesting more than one strengthening mechanism is operative.

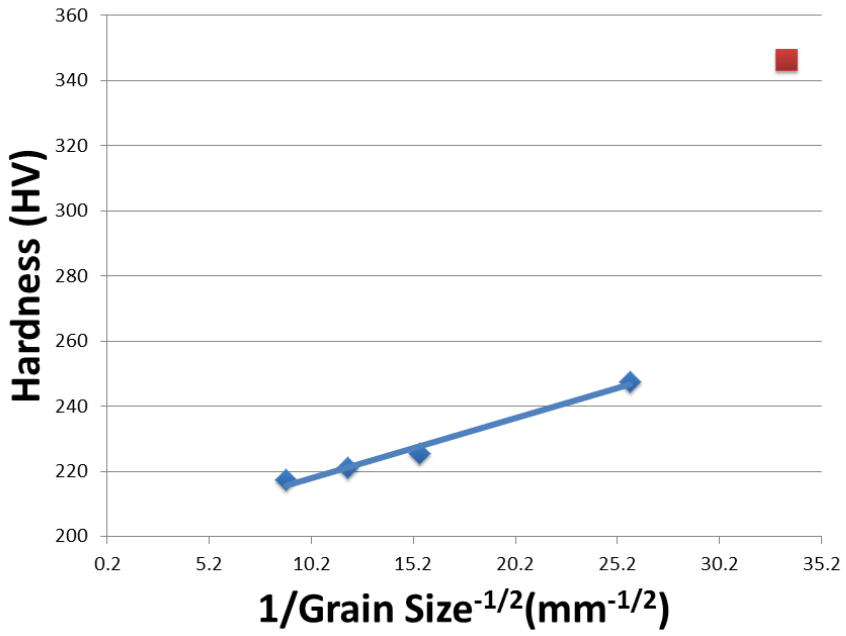

Figure 6. Application of the Hall-Petch equation to SZ hardness values for successful FSW conditions (red square denotes hardness of BM).

Conclusions

This paper examined the correlation between the FSW parameters, tool rotational speed, and tool traverse speed and the resulting welded microstructures and mechanical properties in the ODS steel MA956. Four of eight welding conditions produced defect-free, full penetration welds. Conditions with high thermal input produced defect free welds. The following conclusions are drawn:

(1) Welds with low tool rotational speeds or high tool traverse speeds produce tunnel defects in the weld root or SZ edges. The ratio of tool rotation speed to tool traverse speed can be used as a parameter for predicting defect-free weld consolidation.

(2) Grains in the SZ are substantially coarsened increasing with higher heat input conditions due to dynamic recrystallization.

(3) A persistent, simple torsional texture in the SZ was observed for all FSW conditions.

(4) An abrupt change in grain size and hardness exists across the TMAZ to SZ interface. This change is most pronounced on the advancing side for each welding condition. Higher heat input conditions produce a more abrupt change in both grain size and hardness equating to a smaller but steeper TMAZ.

(5) Hardness decreases from the BM to the SZ by 37% for each welding condition and may be correlated to observed grain growth in the SZ using the Hall-Petch relationship. This suggests that grain coarsening is the dominant, low-temperature strengthening mechanism of the welded material.

Acknowledgements

This work was sponsored by a collaborative research agreement between the Naval Postgraduate School and Lawrence Livermore National Laboratory. Friction stir welding was performed and technical assistance was provided by MegaStir Technologies.

References

[1] E. E. Bloom, S. J. Zinkle, and F. W. Wiffen, "Materials to deliver the promise of fusion power - progress and challenges," *Journal of Nuclear Materials,* vol. 329, pp. 12-19, Aug 1 2004.

[2] S. Ukai, T. Nishida, T. Okuda, and T. Yoshitake, "Development of oxide dispersion strengthened steels for FBR core application, (II) - Morphology improvement by martensite transformation," *Journal of Nuclear Science and Technology,* vol. 35, pp. 294-300, Apr 1998.

[3] M. G. McKimpson and D. Odonnell, "JOINING ODS MATERIALS FOR HIGH-TEMPERATURE APPLICATIONS," *Jom-Journal of the Minerals Metals & Materials Society,* vol. 46, pp. 49-51, Jul 1994.

[4] V. G. Krishnardula, N. I. Sofyan, W. F. Gale, and J. W. Fergus, "Joining of ferritic oxide dispersion strengthened alloys," *Transactions of the Indian Institute of Metals,* vol. 59, pp. 199-203, Apr 2006.

[5] S. Noh, R. Kasada, A. Kimura, S. H. C. Park, and S. Hirano, "Microstructure and mechanical properties of friction stir processed ODS ferritic steels," *Journal of Nuclear Materials,* vol. 417, pp. 245-248, Oct 1 2011.

[6] F. Legendre, S. Poissonnet, P. Bonnaillie, L. Boulanger, and L. Forest, "Some microstructural characterisations in a friction stir welded oxide dispersion strengthened ferritic steel alloy," *Journal of Nuclear Materials,* vol. 386-88, pp. 537-539, Apr 30 2009.

[7] A. Etienne, N. J. Cunningham, Y. Wu, and G. R. Odette, "Effects of friction stir welding and post-weld annealing on nanostructured ferritic alloy," *Materials Science and Technology,* vol. 27, pp. 724-728, Apr 2011.

[8] W. Han, S. Ukai, F. Wan, Y. Sato, B. Leng, H. Numata, N. Oono, S. Hayashi, Q. Tang, and Y. Sugino, "Hardness and Micro-Texture in Friction Stir Welds of a Nanostructured Oxide Dispersion Strengthened Ferritic Steel," *Materials Transactions,* vol. 53, pp. 390-394, Feb 2012.

[9] M. West, B. Jahsthi, P. Hosemann, and V. Sodesetti, "Friction stir welding of oxide dispersion strengthened alloy MA956," in *Friction Stir Welding and Processing VI, TMS*, Warrendale, PA, 2011, pp. 33-40.

[10] J. Wang, W. Yuan, R. S. Mishra, and I. Charit, "Microstructure and mechanical properties of friction stir welded oxide dispersion strengthened alloy," *Journal of Nuclear Materials,* vol. 432, pp. 274-280, 2013.

[11] W. M. Thomas, E. D. Ncholas, J. C. Needham, M. G. Murch, P. Templesmith, and C. J. Dawes, "G.B. Patent Application No. 9125978.8," 1991.

[12] R. S. Mishra and Z. Y. Ma, "Friction stir welding and processing," *Materials Science & Engineering R-Reports,* vol. 50, pp. 1-78, Aug 31 2005.

[13] R. Nandan, T. DebRoy, and H. K. D. H. Bhadeshia, "Recent advances in friction-stir welding - Process, weldment structure and properties," *Progress in Materials Science,* vol. 53, pp. 980-1023, Aug 2008.

[14] U. F. Kocks, C. N. Tome, and H. R. Wenk, *Texture and Anisotropy: Preferred Orientation in Polycrystals and their Effect on Materials Properties*: Cambridge Univesity press, 1998.

[15] W. T. Han, F. R. Wan, B. Leng, S. Ukai, Q. X. Tang, S. Hayashi, J. C. He, and Y. Sugino, "Grain characteristic and texture evolution in friction stir welds of nanostructured oxide dispersion strengthened ferritic steel," *Science and Technology of Welding and Joining,* vol. 16, pp. 690-696, Nov 2011.

[16] S. K. Chimbli, D. J. Medlin, and W. J. Arbegast, *Minimizing lack of consolidation defects in friction stir welds*, 2007.

[17] P. Biswas, D. A. Kumar, and N. R. Mandal, "Friction stir welding of aluminum alloy with varying tool geometry and process parameters," *Proceedings of the Institution of Mechanical Engineers Part B-Journal of Engineering Manufacture,* vol. 226, pp. 641-648, Apr 2012.

[18] R. Nandan, G. G. Roy, T. J. Lienert, and T. DebRoy, "Numerical modelling of 3D plastic flow and heat transfer during friction stir welding of stainless steel," *Science and Technology of Welding and Joining,* vol. 11, pp. 526-537, Sep 2006.

[19] R. D. Doherty, D. A. Hughes, F. J. Humphreys, J. J. Jonas, D. J. Jensen, M. E. Kassner, W. E. King, T. R. McNelley, H. J. McQueen, and A. D. Rollett, "Current issues in recrystallization: a review," *Materials Science and Engineering a-Structural Materials Properties Microstructure and Processing,* vol. 238, pp. 219-274, Nov 15 1997.

[20] M. F. Hupalo, M. Terada, A. M. Kliauga, and A. F. Padilha, "Microstructural characterization of INCOLOY alloy MA 956," *Materialwissenschaft Und Werkstofftechnik,* vol. 34, pp. 505-508, May 2003.